Frequenz, Vol. **65** (2011), pp. 209–215  DOI 10.1515/FREQ.2011.029

# Time-Domain Emission Measurements in K-Band

**Christian Hoffmann**[1,*] **and Peter Russer**[2]

[1] Institute for High Frequency Engineering, Technische Universität München, Munich, Germany
[2] Institute for Nanoelectronics, Technische Universität München, Munich, Germany

**Abstract.** The presented time-domain EMI measurement system allows for full-compliance measurements according to CISPR 16-1-1 in the frequency range from 9 kHz to 26 GHz. With the combination of ultra-fast analog-to-digital-conversion and real-time digital signal processing on a field-programmable-gate-array (FPGA) with ultra-broadband multi-stage down-conversion, time-domain methods are employed for measurements into K-band. This allows for a reduction in scan times by several orders of magnitude. A scan from 9 kHz to 26 GHz with a 9 kHz IF-filter bandwidth is completed in under 200 s, while over $5 \cdot 10^6$ frequency points are calculated. The use of low-loss components and integrated preamplifiers yields an ultra-low system noise floor power spectral density of typically below $-150$ dBm/Hz. The system IF dynamic range of over 60 dB allows for the measurement of high-dynamic range signals like radar pulses. Measurements of the radiated emissions of a personal computer and the non-stationary emissions of a microwave oven are presented.

**Keywords.** Broadband down conversion, electromagnetic compatibility (EMC), electromagnetic interference, time-domain measurements.

**PACS®(2010).** 07.50.Ek, 07.50.Hp, 07.50.Qx.

## 1 Introduction

The measurement of electromagnetic emissions (EMI) is a crucial first step in order to protect modern communication services. Since the first systems have been developed by Siemens and General Electric [1, 2], such measurements have been predominantly done with heterodyne measurement receivers. These instruments provide high sensitivity by use of, frequently external, preamplifiers and high dynamic range by use of a complex preselection. The downside of those systems are the potentially long scan times and the inability to characterize non-stationary EMI.

The presented EMI measurement system employs time-domain methods with fast broadband sampling to reduce scan times by several orders of magnitude. With the presented system, a scan over the complete band from 9 kHz to 26 GHz with an IF bandwidth of 9 kHz takes less than 200 s. With a traditional EMI-receiver, the sequential measurements of over $5{\cdot}10^6$ frequency points with a dwell-time of 100 ms, would take more than one day.

Real-time capability was introduced by a Short-Time-Fast-Fourier-Transform-based spectrogram [3]. It allows for the real-time characterization of non-stationary emitters with a real-time bandwidth of 162.5 MHz. A statistical approach to evaluate fluctuating emissions using the amplitude probability distribution (APD) is introduced in [4].

Although, high-speed analog-to-digital converters (ADC) with a sampling rate of 2.6 GS/s and a nominal dynamic range of 8 bit are used in the system, such a system can only sample input frequencies up to 1.3 GHz without aliasing errors. In order to increase the systems upper frequency limit to values above 1.3 GHz, a multi-stage broadband down-converter was added [5]. The system presented in this paper is further increasing the frequency range up to 26 GHz, covering K-band. With its high sensitivity through low-loss components and integrated preamplifiers and its high dynamic range, it enables for full-compliance measurements in accordance with CISPR-16-1-1 [6] in the frequency range from 9 kHz to 26 GHz. EMI-measurements of a personal computer and of the non-stationary emissions of a microwave oven were conducted in a full-anechoic chamber and are presented.

## 2 Time-Domain Measurement System

Figure 1 shows the block diagram of the presented time-domain EMI measurement system. For measurements below 1.1 GHz, the EMI-Signal is lowpass-filtered to enforce the Nyquist criterion and directly sampled by the multiresolution ADC. The spectrum is weighted by digital detectors and the amplitude spectrum or the spectrogram are displayed.

In the frequency range from 1.1–26 GHz, the input signal is broadbandly down-converted to the range below 1.1 GHz by a cascaded down-converter.

**Corresponding author:** Christian Hoffmann, Institute for High Frequency Engineering, Technische Universität München, Munich, Germany; E-mail: c.hoffmann@tum.de.

Received: June 19, 2011.

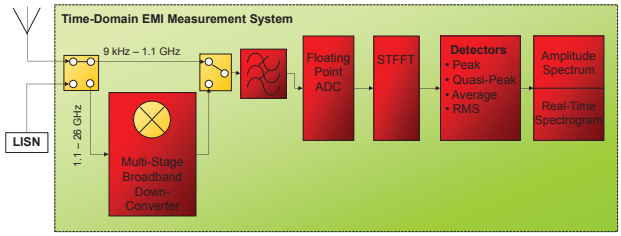


**Figure 1.** Time-Domain EMI Measurement System.

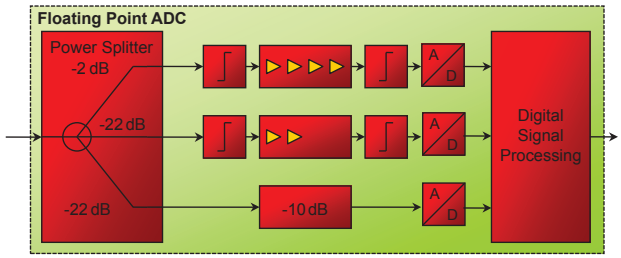


**Figure 2.** Floating-point analog-to-digital converter.

### 2.1 Multiresolution Time-Domain EMI Measurement System

Because the dynamic range of current ADCs with high sampling rate is limited, an arrangement of 3 ADCs is used to increase the dynamic range. In Figure 2, the block diagram of the floating-point ADC is shown [7]. The input signal is distributed into three channels by an asymmetrical power splitter. Two channels consist of limiters, a low-noise amplifier, and an ADC, digitizing the amplitude ranges from 0 to 1.8 mV and from 0 to 200 mV. The third channel consists of an attenuator and an ADC and digitizes the amplitude range from 0 to 5 V. The signal is recorded in all three channels simultaneously.

A floating-point representation is calculated from the data of all three ADCs. The dynamic range is maximized by taking the value from the ADC that shows the maximum value that is not clipped.

### 2.2 Short-Time-Fast-Fourier-Transform

For non-stationary signals, a spectrogram is calculated via the Short-Time-Fast-Fourier-Transform. During the selected dwell-time, a Gaussian window function $w[n]$, corresponding to the IF-filter of a conventional measurement receiver, is shifted in time with a discrete time-coordinate $\tau$. For every value of $\tau$, the momentary spectrum is calculated via FFT. The short-time spectrum $X[\tau, k]$ is calculated by

$$X[\tau,k] = \sum_{n=0}^{N-1} x[n]w[n-\tau]e^{\frac{-j2\pi kn}{N}}, \qquad (1)$$

while $w[n-\tau]$ is the shifted window function and $x[n]$ is the discrete input signal. The calculated spectra over time describe a spectrogram. Mathematically it can be shown that the short-time FFT corresponds to a set of parallel receivers, where the time-domain signal extracted from the spectrogram corresponds to the envelope of the IF-Signal of each receiver [8].

### 2.3 Digital Down-Conversion

In order to avoid data overflow in the signal processor and enable real-time processing of the signal, the frequency range from DC to 1.1 GHz is subdivided into eight subbands with a bandwidth of 162.5 MHz each. For the in-phase and quadrature channel, a polyphase decimation filter reduces the sampling frequency in order to fulfill the Nyquist criterion. Every subband is digitally down-converted to the baseband and the subbands are processed sequentially [7]. The output sampling frequency is 325 MHz, while the bandwidth is 162.5 MHz. The block diagram is shown in Figure 3.

### 2.4 1.1–6 GHz Down-Converter

The block diagram of the 1.1–6 GHz down-converter is shown in Figure 4. The signal is down-converted in two steps by two mixers. This mixing scheme allows for a sufficient suppression of the image band by a single fixed preselection bandpass filter, because the input frequency band

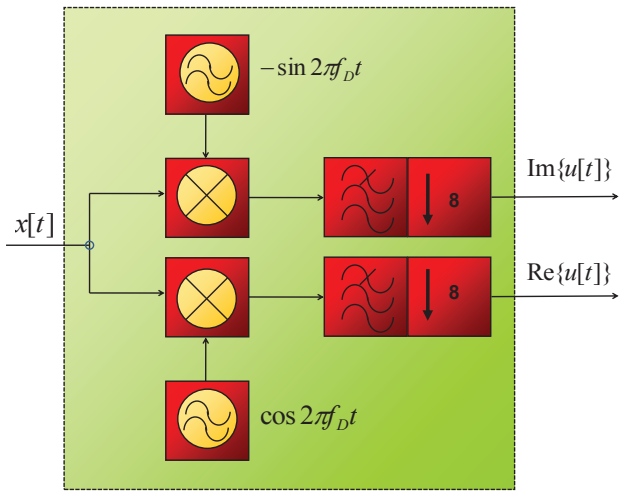


**Figure 3.** Digital down-conversion.

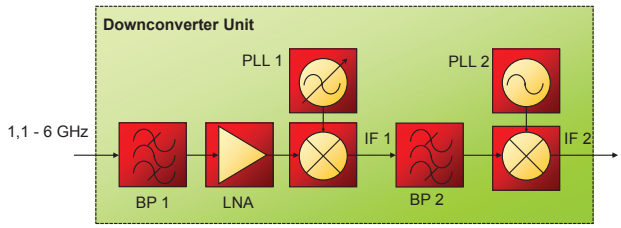


**Figure 4.** 1.1–6 GHz down-converter.

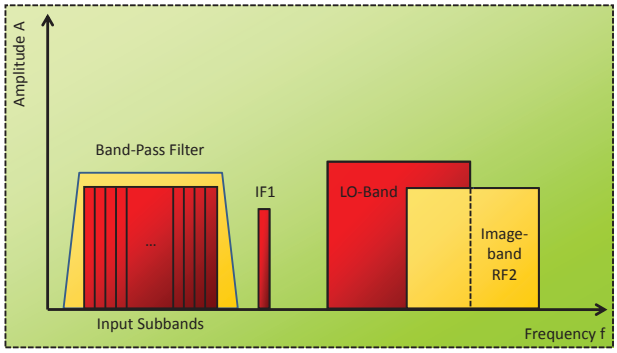


**Figure 5.** Up-conversion frequency bands.

and the image frequency band do not overlap spectrally. The corresponding frequency bands are shown in Figure 5. The input band is divided into 16 subbands with a bandwidth of 325 MHz. The first mixer up-converts the input subbands to a first intermediate frequency band above the input band. The local oscillator frequencies are generated by a low-noise PLL-Synthesizer. A second mixer finally down-converts the IF-band to the frequency band from 9 kHz to 1.1 GHz, where it is sampled and further digitally processed by FFT to compute the amplitude spectrum. The preselection filter suppresses out-of-band narrowband and broadband interference, thus increasing system dynamic range. A low-noise InGaP/GaAs HBT amplifier (LNA) yields a low noise figure and high system sensitivity.

### 2.5 6–26 GHz Down-Converter

A third mixer stage is added to extend the frequency range of the measurement system to 26 GHz. Figure 6 shows the block diagram of the 6–26 GHz down-converter. The preselection consists of 5 bandpass filters, that divide the EMI input signal above 6 GHz into 5 ultra-wide subbands: band 1 from 6–9 GHz, band 2 from 9–13 GHz, band 3 from 13–18 GHz, band 4 from 18–22 GHz and band 5 from 22–26 GHz. The filtered signal is amplified by a low-noise amplifier with high gain and then down-converted to the input frequency range of the 1.1–6 GHz down-converter by a broadband mixer with low conversion loss. The local oscillator frequencies are generated by a low phase noise PLL-Synthesizer.

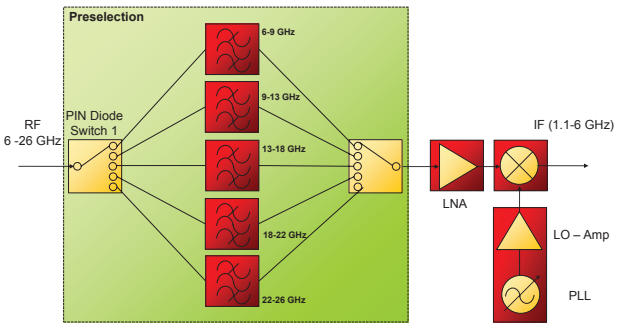


**Figure 6.** 6–26 GHz down-converter.

## 3 Hardware Implementation

The switching between the five preselection bands is done via broadband, low insertion loss single-pole-quintuple-throw (SP5T) PIN-diode switches. PIN-diodes are commonly used in microwave and millimeter wave switches and variable attenuators.

By variation of the stored charge $Q = I_F \cdot \tau$ in the intrinsic region of a PIN-diode, its series resistance $R_S$ can be changed by several orders of magnitude [9] according to

$$R_S = \frac{W^2}{I_F \cdot \tau(\mu_n + \mu_p)}, \tag{2}$$

where $W$ is the width of the intrinsic region, $I_F$ is the forward bias current, $\tau$ is the minority carrier lifetime and $\mu_n$ and $\mu_p$ are the electron and hole mobilities.

For a single matched series diode, insertion loss IL and isolation ISO are determined by

$$\mathrm{IL} = 20\log_{10}\left(1 + \frac{R_S}{2Z_0}\right), \tag{3}$$

$$\mathrm{ISO} = 10\log_{10}\left(1 + \frac{1}{(4\pi f C_t Z_0)^2}\right), \tag{4}$$

with the reference impedance $Z_0$ and the junction capacitance in reversed polarity $C_t$. For a common diode in a beam-lead package and a reference impedance of 50 Ohm, (4) yields an isolation of only around 10 dB at 26 GHz. To increase isolation, a series-shunt configuration is commonly used, were dual shunt-diodes short-circuit the paths in the OFF-state in addition to the series diode in reverse polarity.

Because of the high electron mobility of AlGaAs and the low diode junction capacitance, a AlGaAs SP5T PIN-diode switch chip was employed. To avoid coupling between the paths, a hexagonal shape was chosen for the layout. The switches were fabricated on a glass reinforced hydrocarbon/ceramic RF substrate. The switch is depicted in Figure 7.

The control current is injected via broadband Bias circuits (Bias-Tees). Broadband, low-loss SMD capacitors and conical coils are used. The difference in width between the matched transmission line and the capacitors yields discontinuities with the inherent decrease in the return loss and increase in insertion loss. The bad match also negatively affects the performance of the connected filters and amplifiers and might even lead to instability with conditionally-stable amplifiers. To diminuish this problem, a defected ground structure (DGS) below the discontinuity was designed. The

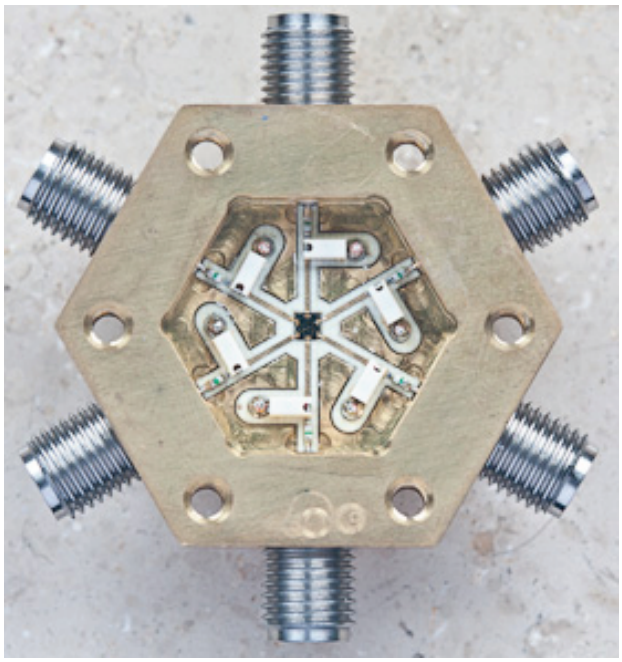

**Figure 7.** SP5T PIN-diode switch.

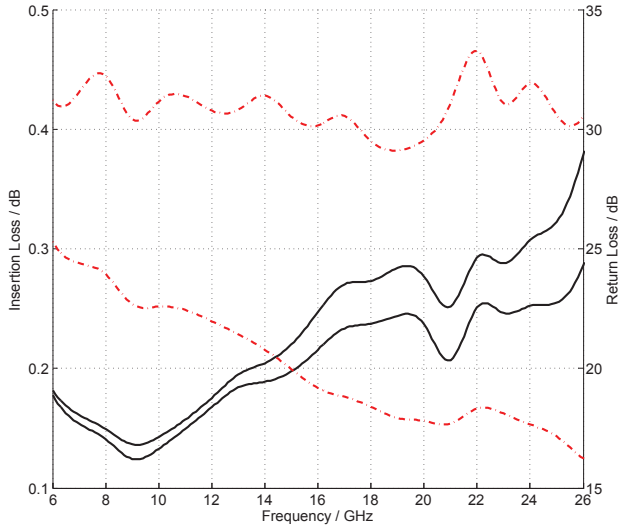


**Figure 8.** Simulated insertion loss (straight line) and return loss (broken line).

characteristic impedance $Z_0$ of a waveguide is determined by its capacitance per unit length $C'$ and its inductance per unit length $L'$ and is defined as $Z_0 = \sqrt{L'/C'}$ for the lossless case. By the insertion of cutouts in the ground-layer below the capacitors, the capacitance per unit length $C'$ is lowered, yielding a matched line despite its greater width. For the simulation and optimization of the Bias-Tee with DGS, a 3D electromagnetic field simulator was used. The simulation results are shown in Figure 8. The return loss is increased by up to 15 dB, while the insertion loss is decreased by about 0.1 dB.

Whenever a circuit is put into a closed metallic cavity, e.g. a housing, electromagnetic field energy might couple to the resonant modes of the cavity. The resonant frequencies of a circular cylindrical metallic cavity are determined by [10]

$$\omega_{\mathrm{mnp}}^{TM_{\mathrm{mnp}}} = \frac{c_0}{\epsilon_r \mu_r} \sqrt{\xi_{\mathrm{nm}}^2 + \left(\frac{p\pi}{d}\right)^2}, \tag{5}$$

$$\omega_{\mathrm{mnp}}^{TE_{\mathrm{mnp}}} = \frac{c_0}{\epsilon_r \mu_r} \sqrt{\xi_{\mathrm{nm}}'^2 + \left(\frac{p\pi}{d}\right)^2}, \tag{6}$$

where $\xi_{\mathrm{nm}}^2$ and $\xi_{\mathrm{nm}}'^2$ are the zeros of the ordinary Bessel function of first kind and of its derivative. To increase the frequency of the dominant mode, the chip was placed into an inner circular cylindrical cavity, which exhibits a dominant mode above 30 GHz. The feeding waveguides and the Bias-Tees were placed in arms, extending from this cavity. As the dominant modes field slightly extends into the arms, the resulting dominant mode frequency of the entire case is lowered to just below 30 GHz. This design ensures the switches resonance free operation from 6–26 GHz.

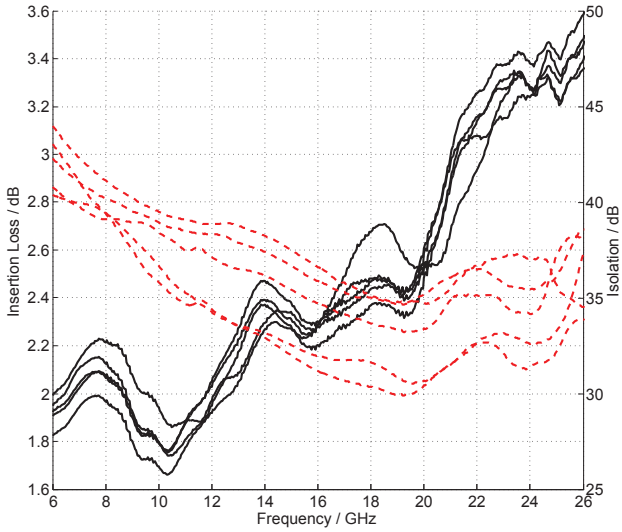


**Figure 9.** Measured insertion loss (straight line) and isolation (broken line).

To characterize the switches performance, the scattering parameters were determined with a Vector Network Analyzer (VNA). The results are given in Figure 9. The insertion loss for all paths stays below 3.6 dB. The isolation exceeds 30 dB over the complete frequency range from 6–26 GHz.

## 4 System Measurements

In order to determine the power spectral density of the system noise floor from 1–26 GHz, the noise voltages $V_N$ were measured at distinct frequencies using the average detector and a matched input and the respective noise power $P_N$ was calculated. As the bandwidth of the used IF-filter with a Gaussian characteristic was 9 kHz, the resulting noise power was normalized to an IF bandwidth of 1 Hz, using

$$P_{\mathrm{NF,AV}} = P_N / B_{\mathrm{ENB,IF}}, \tag{7}$$

where $P_{\mathrm{NF,AV}}$ is the average power of the system noise floor, and $B_{\mathrm{ENB,IF}}$ is the equivalent noise bandwidth of the IF-filter. The results are listed in Table 1. The system exhibits a low noise floor power spectral density of under −150 dBm/Hz over the complete frequency range.

CISPR 16-1-1 requires an IF dynamic range of over 40 dB for measurements above 1 GHz. For the detector calibration in CISPR Band E above 1 GHz, pulse-modulated sinusoidal signals are used. The difference in level between the peak and average detector measurements of a pulse-modulated signal is defined as the IF dynamic range. A pulse generator fed a pulse-modulated sinusoidal signal with a frequency of 25 GHz to the system input. The signal pulse width was set to 1 µs and the pulse period to 40 ms. The spectra are shown in Figure 10. The measurements indicate an IF dynamic range of around 52 dB for an IF bandwidth of 120 kHz. While these measurements were conducted with IF-bandwidths of 120 kHz, the corresponding change of the pulse and noise levels for other filter bandwidths can be calculated by

$$\Delta A_{\mathrm{Pulse}} = 20 \cdot \log_{10}\left(\frac{B_{\mathrm{imp,1}}}{B_{\mathrm{imp,2}}}\right), \tag{8}$$

$$\Delta A_{\mathrm{Noise}} = 10 \cdot \log_{10}\left(\frac{B_{\mathrm{Noise,1}}}{B_{\mathrm{Noise,2}}}\right), \tag{9}$$

where $B_{\mathrm{imp,x}}$ and $B_{\mathrm{Noise,x}}$ are the equivalent impulse and noise bandwidths of the IF-filters. $B_{\mathrm{imp,x}}$ and $B_{\mathrm{Noise,x}}$ are proportional to the IF-filters 3 dB-bandwidths. With a 1 MHz IF-filter, (8) and (9) yield an increase in the displayed pulse level of 18.4 dB and an increase in noise level of 9.2 dB. The IF dynamic range for a 1 MHz IF-filter is then 52 dB + (18.4 dB–9.2 dB) = 61.2 dB. The system IF dynamic range exceeds the CISPR 16-1-1 requirements by over 20 dB.

Modern consumer electronics employing high-speed digital and analog components are prone to interfere with contemporary communication services. In order to protect those services, specific limits for the radiated emissions must not be exceeded. For the characterization of the radiated emissions of a standard personal computer (PC), the PC was placed in a full-anechoic chamber and was measured in a distance of 1 m to the antenna. A broadband quad-ridged horn antenna with a bandwidth from

**Table 1.** Measured Noise Floor Power Spectral Density

| Frequency / MHz | Power Spectral Density / dBm/Hz |
|---|---|
| 1000 | −166.2 |
| 2000 | −166.4 |
| 3000 | −166.9 |
| 4000 | −166.9 |
| 5000 | −166.9 |
| 6000 | −165.6 |
| 7000 | −158.7 |
| 8000 | −158.5 |
| 9000 | −158.5 |
| 10 000 | −158.6 |
| 11 000 | −158.4 |
| 12 000 | −158.0 |
| 13 000 | −157.7 |
| 14 000 | −157.5 |
| 15 000 | −157.4 |
| 16 000 | −154.6 |
| 17 000 | −154.6 |
| 18 000 | −153.8 |
| 19 000 | −153.0 |
| 20 000 | −152.9 |
| 21 000 | −150.2 |
| 22 000 | −150.1 |
| 23 000 | −153.4 |
| 24 000 | −151.1 |
| 25 000 | −150.8 |
| 26 000 | −150.1 |

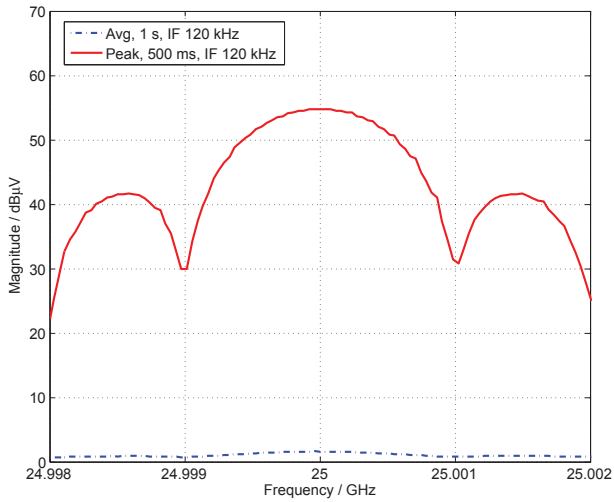


**Figure 10.** Measurement of a pulse-modulated signal.

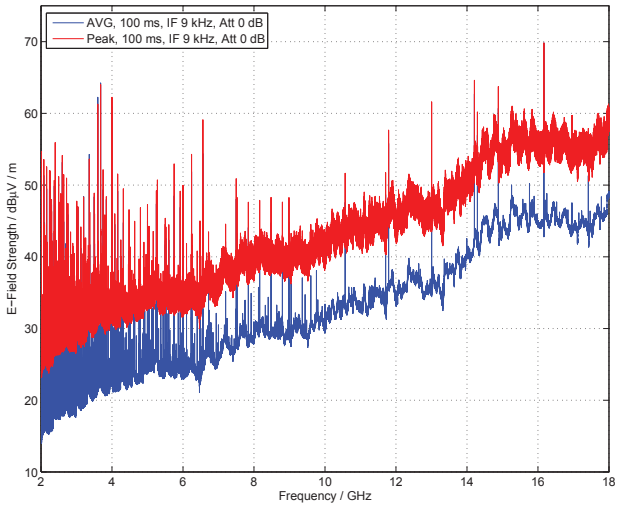


**Figure 11.** Radiated emission spectrum of a personal computer.

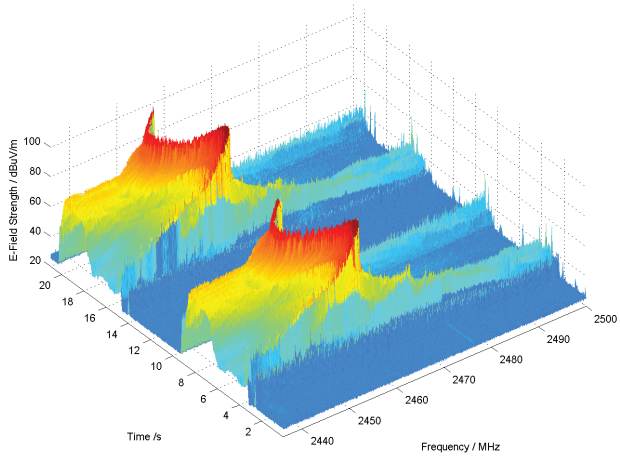


**Figure 12.** Spectrogram of the fundamental of a microwave oven.

1.7–20 GHz [11] was used for the measurements. To compensate for cable losses and to give the electric field strength of the radiated EMI, the corresponding transducer factors and the antenna factor were applied. An IF-filter bandwidth of 9 kHz was used for high sensitivity and the measured spectrum from 2–18 GHz was weighted by the peak and average detectors. At a frequency resolution of 50 kHz, around 320 000 frequency points were calculated, while the scan time was under 150 s. The measurements in Figure 11 show, that the PC emits various narrowband emissions caused e.g. by the central processing unit at 2.4 GHz.

An interesting non-stationary emitter found in almost every household is the microwave oven. The measurements were conducted in a full-anechoic chamber in a distance of 3 m to the antenna. The real-time spectrogram allows for the characterization of the time-behaviour of the magnetrons radiated emissions. The microwave oven was set to a medium power level, were the magnetron periodically turned on and off. The spectrogram in Figure 12 shows the radiated spectrum over a time-period of 20 seconds. At around 4 s the magnetron starts oscillating after a short broadband switching pulse. From around 4–10 s the free-running oscillators frequency drift can be observed.

A similar behaviour can be measured at higher harmonics of the magnetrons fundamental oscillation frequency. The measured spectrogram around the $4^{th}$ harmonic is shown in Figure 13. Although the E-Field strength of the $4^{th}$ harmonic at around 9.83 GHz is around 30 dB lower than the fundamentals, the time-domain EMI measurement system with its high sensitivity and low noise floor allows for the evaluation of of the time-behaviour of the radiated EMI.

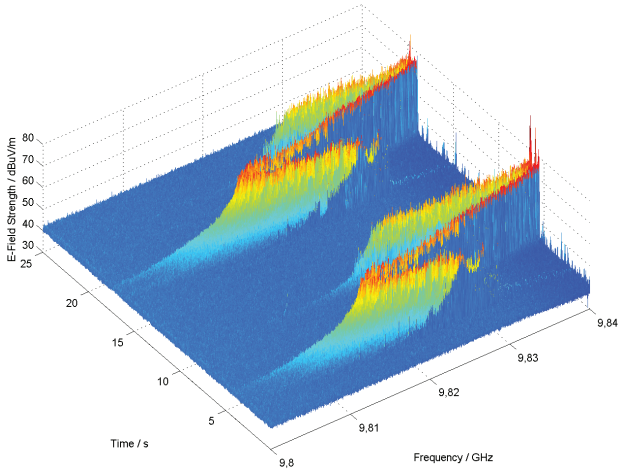


**Figure 13.** Spectrogram of the $4^{th}$ harmonic of a microwave oven.

## 5 Conclusion

A time-domain system for fast and accurate EMI measurements from 9 kHz to 26 GHz was presented. The system fulfills all requirements for full-compliance measurements according to CISPR 16-1-1. With its integrated preamplifiers and preselection filters, the system exhibits an ultra-low noise floor power spectral density of typically below −150 dBm/Hz and a very high IF dynamic range in excess of 60 dB. Measurements of electronic consumer devices and electric household appliances were conducted and show that non-stationary emitters can be characterized with high sensitivity.

**Acknowledgments**

The authors would like to thank the Bayerische Forschungsstiftung and GAUSS INSTRUMENTS GmbH, Munich, Germany for funding this project.

**References**

[1] C. R. Barhydt, “Radio Noise Meter and its Application”, *General Electric Rev.*, Vol. 36. pp. 201–205, 1933.

[2] K. Hagenhaus, “Die Messung von Funkstörungen”, *Elektrotechnische Zeitschrift*, Vol. 63. pp. 182–187, 1942.

[3] S. Braun, M. Al-Qedra, P. Russer, “A novel Realtime Time-domain Measurement System based on Field Programmable Gate Arrays”, 17$^{th}$ *International Zurich Symposium On Electromagnetic Compatibility, Singapore, Singapore*, pp. 501–504, 2006.

[4] H. H. Slim, C. Hoffmann, S. Braun, P. Russer, “A novel Multichannel Amplitude-Probability-Distribution for a time-domain EMI Measurement System According to CISPR 16-1-1”, *EMC Europe 2011*, 2011.

[5] C. Hoffmann, P. Russer, “A Time-Domain System for EMI Measurements above 1 GHz with High Sensitivity”, *German Microwave Conference 2011, Darmstadt, Germany*, March 2011.

[6] CISPR 16-1-1, Ed. 3.1 Am. 1, “Specification for radio disturbance and immunity measuring apparatus and methods Part 1-1: Radio disturbance and immunity measuring apparatus – Measuring apparatus”, *International Electrotechnical Commission*, 2010.

[7] S. Braun, S. Alt, P. Russer, "A novel multiresolution high-dynamic ultra-broadband time-domain EMI measurement system," *Microwave Symposium Digest, 2005 IEEE MTT-S International*, 4 pp., 2005.

[8] J. Allen, “Short term spectral analysis, synthesis, and modification by discrete Fourier transform”, *IEEE Transactions on Acoustics, Speech and Signal Processing*, vol. 25, pp. 235–238, 1977.

[9] S. M. Sze, “Modern Semiconductor Device Physics”, John Wiley & Sons, 1988

[10] P. Russer, “Electromagnetics, Microwave Circuit and Antenna Design for Communications Engineering”, Second Edition, Artech House, 2006

[11] RF Spin, Broadband Quad-Ridged Horn Antenna QRH20, Data Sheet